Contents lists available at SciOpen

Food Science and Human Wellness

journal homepage: https://www.sciopen.com/journal/2097-0765

China Food Publishing Co.

# Albumen/gelatin bio-inks preparation in 3D bio-printing for *in situ* tissue culture of cultured meat

Xiang Guo[a,b], Feng Yang[a], Yu Qi[a], Yingying Li[a], Shouwei Wang[a,*], Baohua Kong[b,*]

[a] China Meat Research Center, Beijing 100068, China
[b] College of Food Science, Northeast Agricultural University, Harbin 150030, China

ARTICLE INFO

*Article history:*
Received 21 February 2024
Received in revised form 6 March 2024
Accepted 25 March 2024

*Keywords:*
3D bio-printing
Bio-ink
Tissue culture
Protein interaction

ABSTRACT

Three-dimensional (3D) bio-printing is an emerging tissue engineering technology, and its printing parameters have been upgraded to enable in-depth application in cell-cultured meat. However, excellent printable and edible bio-inks for cell-cultured meat are in urgent need of development. Therefore, a low-cost bio-ink based on albumin and gelatin was developed. At first, suitable printability of the bio-ink was determined by rheology analysis, excellent mechanical stability, and excellent mechanical stability of the printed scaffold was also proved by water absorption and degradation rate. Next, the biocompatibility of the scaffold and its interaction with cells were clarified through cell proliferation culture, cell status research and omics analysis. Notably, AG7 demonstrated better printability and AGS7 provided better conditions for cell attachment, proliferation and migration, S-shaped exponential growth curve further revealed the significant advantages of AGS7 scaffolds in cell culture. More importantly, the tissue culture process of muscle cells was simulated to organoid culture, which elucidated the interaction information between cells and scaffolds. This work has filled the vacancy in the industry and provides a novel strategy for the development of production of cell cultured meat.



## 1. Introduction

Cell cultured meat, also known as biologically cultured meat, is a disruptive meat production technology that has surfaced recently[1-4]. Most of the current cultured -meat comes in the form of minced meat, it is widely believed that constructing three-dimensional (3D) muscle tissue with tissue engineering techniques could be a satisfactory solution[5-7]. 3D bio-printing as a universal engineering technology could be used to acquire 3D constructs with specific structures and shapes. The position of cells and biomaterials can be precisely controlled by computer-aided design, an artificial tissue structure similar to natural tissue can be quickly generated layer by layer[8-12]. Although the development of 3D bio-printing shows great promise in the construction of artificial tissues, poor printability and edibility of bio-ink limited the application of 3D printing in cell cultured meat area, which are easily caused unstable structure formation and bio-risk. In addition, the effects of cell attachment, proliferation and migration are also closely related to the performance of bio-ink. Therefore, it is essential to develop bio-inks with impressive printability and biocompatibility for fabricating ideal 3D muscle tissues[13].

According to some recent research, albumen is an edible and cheap biomacromolecule, which is benefit to cell adhesion and proliferation owing to a variety of components such as ovalbumin, ovotransferrin, ovomucoid, etc.[14-16], which could improve the overall biocompatibility of the prepared scaffold and promote cell proliferation and adhesion. Thus, albumen could be considered as an available material for bio-ink preparation[17]. However, because of high moisture content and chemical instability, albumen is not printable and need to be used with other ingredients[18-20]. Gelatin is a kind of well-known macromolecular hydrophilic colloid, which is the product of partial hydrolysis of collagen. Due to the suitable

* Corresponding authors.
*E-mail address*: cmrc_wsw@126.com (S.W. Wang); kongbh63@hotmail.com (B.H. Kong)
Peer review under responsibility of Beijing Academy of Food Sciences.

SciOpen Publishing services by Tsinghua University Press

http://doi.org/10.26599/FSHW.2024.9250249

rheological property and excellent biocompatibility, gelatin is widely used in extrusion-based 3D bio-printing for making cell scaffold[21-25]. But unfortunately, gelatin demonstrate a sensitive temperature-based phase transition property, which easily transforms from gel to solution when the temperature increases to 25−35 °C. Such a behavior remains a significant challenge for structural retention of scaffold. Therefore, the cross-linking through physical or chemical methods to improve the stability are necessary for gelatin-based scaffold[26-28].

In this study, as shown in Fig. 1A, an emerging composite ink was prepared by mixing gelatin solution with albumen. And a scaffold was prepared through 3D printing. After printing, glutaraldehyde was used at a low concentration for scaffold formation, further enhancing scaffold stability by reacting with the ε-amino groups of lysine and hydroxylysine residues to form Schiff bases. The suitable printability of the ink was assessed by rheological analysis, which studied the storage modulus ($G'$), loss modulus ($G''$), and shear-thinning behavior. The printing ability of the ink was further evaluated through printability. The mechanical stability was assessed by water absorption and degradation rate. Finally, the biocompatibility of the scaffold and its interaction with cells were assessed through cell proliferation culture, cell status research and omics analysis for applying to tissue culture of muscle cells. The presented work provides a new approach to producing cell-cultured meat using 3D bio-printed scaffolds.

## 2. Materials and methods

### 2.1 Materials

#### 2.1.1 Materials and reagents

Glutaraldehyde solution (25%) were purchased from Aladdin Co., Ltd. (China). Fetal bovine serum (FBS, Gibco) was purchased from Thermo Fisher Scientific Inc. (USA). Phosphate buffered solution (PBS), trypsin-EDTA solution (0.25%, T1300), penicillin-streptomycin solution (P/S), paraformaldehyde (4%), Triton X-100, FITC Phalloidin, 4′,6-diamidino-2-phenylindole (DAPI), calcein-AM, propidium iodide (PI) and dulbecco's modified eagle medium (DMEM) were purchased from Solarbio Co., Ltd. (China).

#### 2.1.2 Cell line

The cells used in this experiment were chicken myoblasts. Primary myoblasts were obtained from the leg muscle tissue of 18-day-old chicken embryos by enzymatic digestion.

### 2.2 Preparation of inks

Fresh brown shell eggs (50−65 g) were randomly purchased from local food supermarkets, all eggs come from Beijing white feather chicken, and the albumen was carefully separated from the egg yolk. Gelatin solutions were prepared by dissolving gelatin in water at 40 °C for 2 h (2.5%, 5%, 7.5%, and 10%, *m*/*m*). The separated albumen and gelatin solution were mixed at a volume of 1:1 and stirred well to obtain consistent solutions named AG2, AG5, AG7, and AG10. The prepared solutions were stored at 4 °C for later characterizations. Specific parameters were shown in Table S1.

### 2.3 Rheological analysis of prepared inks

The viscosity and viscoelasticity of inks were assessed by a rheometer (MCR92, Anton Paar Co., Austria). Briefly, the temperature was raised from 4 to 40 °C by temperature sweeping (oscillating mode) at a heating rate of 1 °C/min, and the angular frequency and shear stress were kept at 10 rad/s and 1%, respectively, to obtain $G'$ and $G''$ of inks. Moreover, the viscosity change of inks was evaluated by increasing the shear rate from 0.1 to 100 $s^{-1}$ at 15 °C.

### 2.4 3D printing

Scaffold printing was performed using a bio-printer (SUNP BIOMAKER 2i, Sunp Biotech, China). The printing speed was 5.00 mm/s, the extrusion speed was 4.00 $mm^3$/s, the distance was 0.50 mm, the Bed TEMP was 4 °C, and the nozzle diameter was 22 G (inner diameter 400 μm). The 3D printed scaffolds were prepared according to the above parameters, and each scaffold was printed as a grid structure (2 cm × 2 cm, 4 layers). After printing, 0.25% glutaraldehyde solution was used for cross-linking for 10 min, and then excess glutaraldehyde was washed off with PBS buffer for 3 times.

### 2.5 Printability tests

The printability (Pr) was assessed to ascertain the shape precision of each construct printed with respective inks. The Pr was determined by equation (1):

$$\mathrm{Pr} = \frac{L^2}{16A} \tag{1}$$

Where $L$ represents the perimeter of the pore, and $A$ represents the area of the pore. For this analysis, random images of the printed structure were captured using a microscope (ECLIPSE Ti2, Nikon, Japan). Images were selected for Pr analysis, and printability was calculated by determining the area and perimeter of each pore ($n$ = 10) from optical micrographs using ImageJ software. The homogeneity of the printed features was assessed by measuring the sizes through image analysis.

### 2.6 Scanning electronic microscope (SEM)

In order to characterize the micro-morphology of the scaffold before and after cross-linking, the samples were freeze-dried, and the dried samples were gold-plated under vacuum, and then the samples were examined using a scanning electron microscope (SU8020, Hitachi, Japan) at an operating voltage of 15 kV.

### 2.7 Degradation rate

Scaffold sample with size of 10 mm × 10 mm × 2 mm were prepared. Then the sample was placed in a 6-well plate, containing 3 mL of PBS buffer per well. The sample was cultured at 37 °C for different periods until the sample completely degraded. The degradation rate was calculated by equation (2):

$$R\,(\%) = \frac{W_t - W_0}{W_t} \times 100 \tag{2}$$

Where $W_t$ (g) represent not soaked Scaffold weight, and $W_0$ (g) represent soaked Scaffold weight.

### 2.8 Water holding capacity (WHC)

After the scaffold was formed, the samples were washed with PBS buffer for 15 min, then weighed using an electronic scale, and the WHC of the samples was determined according to the following formula (3):

$$\text{WHC}\ (\%) = \frac{M_W - M_d}{M_d} \times 100 \quad (3)$$

Where $M_W$ (g) represents the washed scaffold wet weight, and $M_d$ (g) represents the scaffold freeze-dried dry weight.

### 2.9 Cell culture

Myoblasts lines were maintained in a growth medium (DMEM supplemented with 10% FBS and 1% antibiotic solution) and incubated at 37 °C in a 5% $CO_2$ atmosphere. Cells were cultured until the confluence reached approximately 80%, dissociated with 0.25% trypsin-EDTA, centrifuged and resuspended in growth medium.

### 2.10 Cell culturing in the 3D scaffold

Bio-inks were prepared by mixing collected cells with each ink at a cell density of $1 \times 10^6$ cells/mL, and scaffolds were then fabricated. The printed cell-laden constructs were incubated in a growth medium at 37 °C under 5% $CO_2$. Two types of cell culture methods were employed. In the first type, known as attached culture, after the preparation of the 3D bio-printing scaffold, the growth medium (15 mL) was directly added to the culture dish for cell culture. In the second type, referred to as suspension culture, the scaffold was separated from the culture dish using a cell scraper, and excess growth medium (30 mL) was added to suspend the scaffold in the culture medium for cell culture. All cells were grown in an incubator (Heracell VIOS 160i, Thermo Fisher, USA) at 37 °C and 5% $CO_2$.

### 2.11 Cell proliferation

Evaluation of cell proliferation was performed using the CCK-8 kit (Solarbio, China). Incubate at 37 °C and 5% $CO_2$ in an incubator. CCK-8 assays were performed on days 1, 2, 3, 4, 5, 6, and 7 to determine cell proliferation in scaffolds. Plates were removed on the corresponding days after incubation, and 10 μL of CCK-8 solution was added. After a 4-h incubation period, 100 μL of the corresponding fraction was removed, and finally the absorbance was recorded at 450 nm using a micro plate reader (Synergy™ H4 Ti2, Bio Tek, USA).

### 2.12 Immunofluorescence

Live/dead assays were performed with Calcein-AM and PI stains. Cut the scaffold material with cells cultured for 7 days into a 1 cm × 1 cm square, place it in a 6-well plate, and suspend it in 2 mL assay Buffer. Stain the scaffolds with calcein-AM/PI solution (1 and 3 μL) for 15 min in the dark. The sample was washed with PBS and observed under a fluorescence microscope (ECLIPSE Ti2, Nikon, Japan).

After a PBS wash, the scaffolds were fixed for ten minutes in 4% paraformaldehyde. Subsequently, the scaffolds were permeabilized for 10 min using 0.5% (*V/V*) Triton X-100 in PBS. The liquid was removed and FITC Phalloidin peptide was added for cytoskeletal staining for 30 min. Finally, add DAPI to stain the nucleus for 15 min. Remove the solution and rinse with PBS for 3 times, then place under the microscope (ECLIPSE Ti2, Nikon, Japan) for observation.

### 2.13 Quantitative real-time PCR analysis

RNA was extracted using the RNeasy Mini Kit (Qiagen, Germany) according to the manufacturer's instructions. The RNA was tested for purity by an ultramicro ultraviolet spectrophotometer (NanoDrop One, Thermo Fisher, USA) adjusted to a uniform concentration. After RNA was reverse transcribed to cDNA using the PrimeScriptTM RT kit (TaKaRa, Japan), quantitative reverse transcription PCR (qRT-PCR) was performed. The reaction was assessed on a Real-Time PCR Instrument (LightCycler 480 II, Roche, USA) detection system. The results were analyzed using the $2^{-\Delta\Delta CT}$ technique, with *GAPDH* utilized as the housekeeping gene for normalization. Primer sequences were performed in Table 1.

**Table 1**
Real-time PCR primers.

| Gene | Primer sequence | Product length (bp) | Melting temperature (°C) |
|---|---|---|---|
| *GAPDH* | F: GGAGAAACCAGCCAAGTAT<br>R: CCATTGAAGTCACAGGAGA | 117 | 55.43<br>54.08 |
| *Ltbp2* | F: CTGGCACAAACCACTGCATC<br>R: GGTGGGTGGTACTCTTGCTC | 148 | 60.04<br>60.04 |
| *Cdh20* | F: GAACCTGGGTCCTTTCCGAG<br>R: CTCAGGCACCTCCACAAAGT | 106 | 60.04<br>59.89 |
| *Megf10* | F: CGTACCAGTACTGCCATCCC<br>R: GCACTAGCAGGAAGAGCACA | 94 | 59.90<br>60.04 |
| *Dsg2* | F: AATCGAAGTGGCAGGAGTGG<br>R: CCGTCCATTCTCGCTTCTGT | 70 | 60.04<br>60.11 |
| *Fgf7* | F: CCCTGAGCGACATACCAGAAG<br>R: GTTGTTTGCTTCTCTCGTCCC | 136 | 60.20<br>59.47 |
| *Bmp4* | F: TTATGCCAAGTCCTGCTGGG<br>R: TTCATGGCTTTGGGCAGAGT | 123 | 60.03<br>59.89 |
| *Pax7* | F: CTGCAGGTACCAAGAGACGG<br>R: CTCCCAGCTGAACATCCCAG | 136 | 60.11<br>60.11 |
| *Myod* | F: CCCATGGAAATGACGGAGGG<br>R: TGAAGCACGGGTCGTCATAG | 73 | 60.47<br>59.83 |
| *Myog* | F: CCTCCATCGTGGAGAGCATC<br>R: CAGTTTTGGACCCGCTCCT | 70 | 59.97<br>59.93 |
| *Ttk* | F: GATGTGGTGCAGAAGACGGA<br>R: AAGGGTGGAATCAAGGCTGT | 92 | 60.04<br>59.22 |
| *Cdk1* | F: GGATGCAAGGCTGTACCTCA<br>R: TCTTAACACGCGAACGATCCA | 104 | 59.75<br>60.07 |
| *Map3k8* | F: TCGGATGTGCTCCTGTTTCC<br>R: CCTTCCCAAAAGCTCCTCGT | 82 | 60.04<br>59.96 |
| *Lgr5* | F: GTTCCCCACTGCTATCAGGAC<br>R: GGATTACCTACAAACGCACGC | 129 | 60.13<br>59.94 |
| *Nid2* | F: CTCACGTTCGACCCCTTCTC<br>R: AACGTGCACTCCAGCTTCTT | 71 | 60.11<br>60.18 |

### 2.14 Western blot

Western blotting was performed to assess the expression of PAX7, MYOD and *β*-tubulin. Proteins were first extracted by a mixture

containing RIPA lysis buffer (Epizyme, GRF101, China). Protein quantification was performed using a BCA kit (Applygen, China). Proteins were separated by 10% SDS-PAGE gel and subsequently transferred to a PVDF membrane (Immobilon, IPVH00010, USA). The blots were first treated for 1 h in 5% nonfat dry milk in TBST and incubated with primary antibodies at 4 °C: rabbit anti-PAX7 (Thermo Fisher, dilution 1/500), mouse anti-MYOD (Santa Cruz, dilution 1/1 000) and rabbit anti-$\beta$-tubulin (Proteintech, dilution 1/5 000) overnight. Then incubated for 2 h with secondary antibodies: anti-Mouse IgG (abclonal, dilution 1/ 5 000), anti-Rabbit IgG (ABclonal, dilution 1/5 000). Immunoblots were detected with the Tanon-5200 Chemiluminescent Imaging System (Tanon, China).

### 2.15 Metabolomics

The TRlzol Reagent (Life Technologies, USA) instruction manual was followed in order to extract the total RNA. Utilizing NanoDrop 2000 (Thermo Fisher Scientific, USA), the concentration and purity of RNA were ascertained. The integrity of the RNA was assessed using the Agilent Bioanalyzer 2100 system's (Agilent Technologies, USA) RNA Nano 6000 assay kit. In accordance with the manufacturer's instructions, sequencing libraries were created using the Hieff NGS Ultima Dual-mode mRNA Library Prep Kit for Illumina (Yeasen Biotechnology, China), and index codes were added to each sample to identify its sequences. The libraries were sequenced on an Illumina NovaSeq platform in accordance with the manufacturer's instructions. The raw reads were further processed with a bioinformatic pipelinetool, BMKCloud (www.biocloud.net) online platform. The raw data in Fastq format was initially processed through internal Perl script, resulting in the extraction of clean data. The valid data were subsequently aligned to a reference genome sequence for further analysis and annotation using the Hisat2 tool software. The gene functions were annotated using the following databases: KO (Kyoto Encyclopedia of Genes and Genomes (KEGG) Ortholog database); GO (Gene Ontology); KOG/COG (Clusters of Orthologous Groups of proteins); Pfam (Protein Family); Nr (NCBI Non-redundant Protein Sequences). The edgeR was used to analyse the differential expression of two samples. The substantially differential expression criterion was chosen at false discovery rate (FDR) < 0.01 and fold change (FC) ≥ 2. GO enrichment analysis was conducted with the clusterProfiler package based on the Wallenius non-central hypergeometric distribution. The statistical enrichment in KEGG pathways was tested using the KOBAS database and clusterProfiler software. The sequences of the differential genes were aligned (blastx) to the genomes of related species (whose protein-protein interactions are present in the STRING database: http://string-db.org/) to obtain the predicted protein-protein interactions (PPIs) of these differential genes. Following that, the PPIs of these differential genes were visualized in Cytoscape.

### 2.16 Statistical analysis

Image processing was performed using ImageJ, and statistical analysis was conducted using GraphPad Prism 10 (USA). The mean ± standard deviation for the 3 replicates was provided with the data. To assess significant differences between the groups, one-way ANOVA approach with the Tukey-Kramer test was employed, and results with a $P$-value of less than 0.05 were considered significant.

## 3. Results and discussion

### 3.1 Rheological analysis of inks

In order to prepare inks for printing, pure albumen obtained from fresh eggs and gelatin solutions with different concentrations (2.5%, 5.0%, 7.5%, and 10.0%, *m*/*m*) were agitated to achieve a uniform liquid consistency for later characterizations. The rheological properties of prepared inks were estimated by rheological analysis primarily. Generally, ink needs to have shear-thinning property to reduce damage to cells during the extrusion process. Therefore, the viscosity of inks at different shear rates was tested. As shown Fig. 1B$_1$, all viscosity of inks held a decreased tendency with increased shear rate from 0.1 to 100 $s^{-1}$, demonstrating a typical shear-thinning property. Such a property renders the ink reducing cell damage during extrusion printing through a nozzle. In addition, the viscosity of the ink significantly increased with an augmentation in gelatin content, which attributed to intertwining and entanglement of gelatin molecular chains within the solution.

Moreover, in order to ensure the mechanical stability of scaffold after printing, the viscoelasticity of inks was also tested. As shown in Figs. 1B$_2$ and B$_3$, the $G'$ and $G''$ of all inks were characterized over a temperature ranged from 4 °C to 40 °C. The $G'$ of all inks consistently exceeded the $G''$ over the entire temperature range, indicating the maintenance of a stable gel-like state. In addition, it is noteworthy that the $G'$ of AG5, AG7, and AG10 exhibited a pronounced decline at 15 °C approximately, which attributed to the weaken hydrogen bonds among gelatin molecules when temperature rises. This result indicated that higher concentrations of gelatin contribute to enhanced stability of ink.

### 3.2 Preparation and characterizations of 3D-printed scaffolds

According to rheological analysis, the shear-thinning property and mechanical stability of prepared inks were confirmed. Subsequently, inks were used for 3D printing to construct scaffold. Briefly, prepared inks were loaded into a syringe for 3D printing, glutaraldehyde solution with low concentration (0.25%, *m*/*m*) was added for cross-linking, and a series of scaffolds named AGS2, AGS5, AGS7, and AGS10 were successfully acquired for subsequent characterizations.

SEM was used to investigate the surface and internal morphology of all scaffolds. As shown in Fig. 1C, the surface morphologies of all scaffolds exhibited a stable single-layer sheet structure after cross-linked with glutaraldehyde, and the interior scaffold demonstrated porous structures. According to the measurements, as shown in Fig. S1, the internal pore size of the scaffold significantly decreased with the increase in gelatin content, which was mainly attributed to the increased viscosity caused by the promoted concentration of gelatin solution. Higher viscosity would prevent the formation of ice crystals in ink lyophilization, thus limiting the size of the pores[29-30]. Notably, such porous structures could facilitate cellular nutrient exchange, proliferation, and migration, thereby contributing to tissue formation[31]. Moreover, cross-linked with glutaraldehyde solution can maintain the shape and structure of the scaffold and improve the mechanical stability of the scaffold in cell culture.

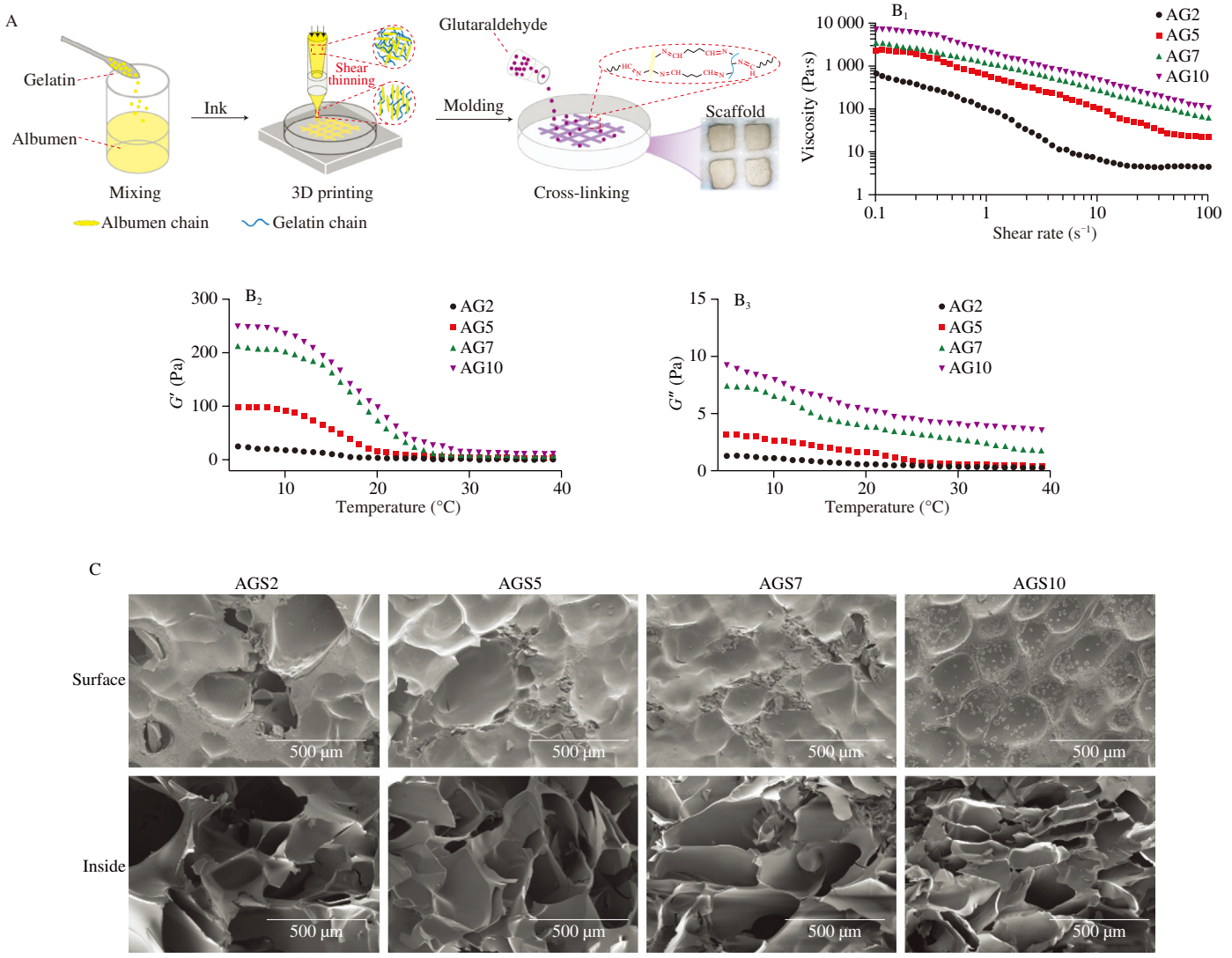


**Fig. 1** (A) Schematic representation of albumen/gelatin ink preparation and 3D scaffold printing and cross-linking. (B) Rheological properties of various inks. ($B_1$) Viscosity of different hydrogel samples at shear rates ranging from 0.1 to 100 $s^{-1}$; ($B_2$) $G'$ and ($B_3$) $G''$ of the tested bio-inks. The temperature was changed as follows: from 4 to 40 °C, rate of 1 °C/min. (C) SEM images of 3D printed scaffolds.

As shown in Fig. 2A, various bio-inks were employed to construct 3D structures by an extrusion-based 3D printer. Since continuous and uniform features with fine chains and pores are crucial for 3D bio-printing, the printability and uniformity of structures printed with each bio-ink were evaluated. Pr values approaching 1 indicates the suitability of the respective bio-inks for 3D printing, facilitating the creation of intricately detailed constructs. Conversely, Pr values below or above 1 indicates inadequate printing[9]. As shown in Fig. 2B, the Pr values of the printed structures exhibited a gradual increase from 0.76 to 1.19 with the escalation of gelatin content. Notably, AGS7 displayed a Pr value nearing 1, indicating the favorable impact of gelatin on enhancing printability to a certain degree. Furthermore, the thickness distribution of all scaffolds was measured to characterize the uniformity of the constructs printed with various bio-inks. As shown in Fig. 2C, the thickness of bio-ink-printed strands initially decreased, and subsequently increased. Additionally, lower distribution and a strand thickness closer to the printhead diameter were exhibited by the AG7, contributing to uniform extrusion and higher print quality. In summary, the results indicated that AG7 bio-ink exhibited superior printing performance, and an appropriate increase of gelatin content has a positive effect on improving the printability and uniformity of bio-ink.

Hygroscopicity plays a pivotal role in mediating the exchange of water-soluble substances, cell viability, and metabolic processes[32]. As illustrated in Fig. 2D, all scaffolds demonstrated a substantial capacity for water absorption. AGS2 and AGS10 displayed the most and the least pronounced swelling ratio respectively, which primarily attributed to the difference between their internal pore sizes. In addition, in order to continuously provide an environment for growth of cells, the stability of scaffold should be estimated. As shown in Fig. 2E, the degradability of each scaffold in PBS buffer was evaluated. Within the initial 5−10 days, due to the dissolution of uncross-linked gelatin and albumen within the scaffold matrix, all scaffolds demonstrated an accelerated degradation behavior, and the rate of mass loss slowed down between 10 and 40 days. Notably, AGS2 exhibited the maximum loss of structural integrity, and AGS10 exhibited the minimum loss of structural integrity in PBS until 40 days. Such results indicated that high-concentration gelatin

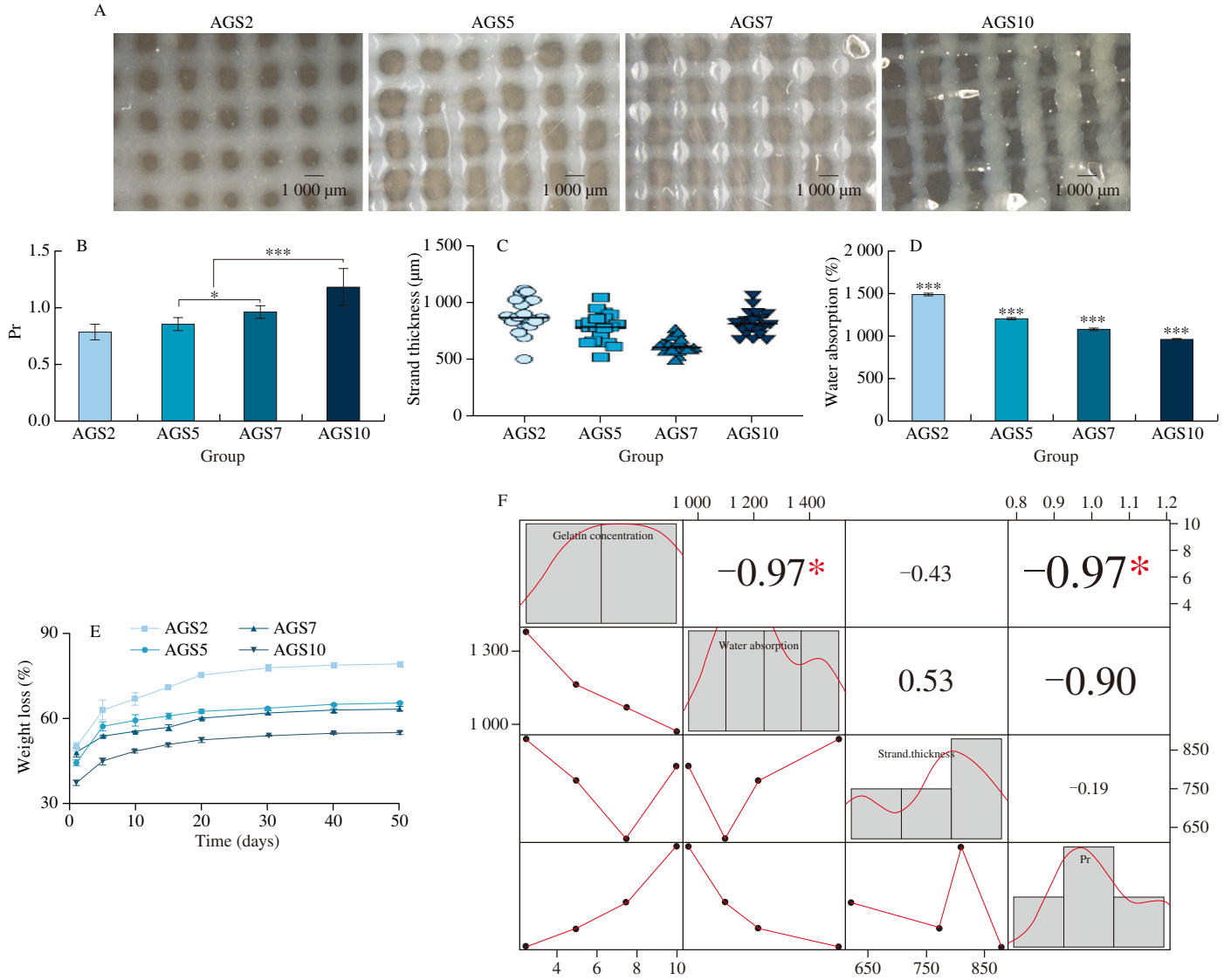


**Fig. 2** 3D printing using various inks, and assessing the mechanical properties of 3D printed scaffolds. (A) Optical images of the printed grid constructs. (B) Printability. Statistical significance was set to $^{***}P < 0.001$ and $^{*}P < 0.05$. (C) Strand thickness of the printed constructs. (D) 3D printed scaffolds water absorption ability. Statistical significance was set to $^{***}P < 0.001$. (E) 3D printing scaffold weight loss rate. (F) Correlation analysis of gelatin concentration, water absorption, printability and strand thickness.

solution was more conductive to cross-linking with glutaraldehyde. As shown in Fig. 2F, it was observed that there was a significant negative correlation (−0.97) between water absorption and the increase in gelatin concentration, while a significant positive correlation (0.97) was found between printing performance and the increase in gelatin concentration. At the same time, it was observed that correlation curves were linear, further indicating that as the gelatin concentration increased, the water absorption decreased while the printing ability increased. It is worth noting that better printing performance was observed when the Pr value was closer to 1, further demonstrating that the printing performance of bio-ink can be improved by appropriately increasing the gelatin concentration

### *3.3 Myoblast bio-printing and cell culture*

Based on the results of the printability and stability evaluations, the AGS5, AGS7, and AGS10 bio-inks were selected for further myoblast printing studies. Cell proliferation and cellular activity in bio-inks during 3D culture was the fundamental issue in evaluating bio-inks. To evaluate the biocompatibility of the 3D bio-printed scaffolds, the live/dead cell staining results of the scaffolds after 7 days were examined, and the cell proliferation behavior was monitored from day 1 to day 7 using the CKK-8 assay. As shown in Fig. 3A, all scaffolds exhibited exceptional biocompatibility, with the proportion of viable cells close to 98% being achieved. In particular, the cells in AGS5 and AGS7 were more uniformly distributed compared to AGS10 and these 2 groups had a more pronounced spindle shape in terms of cell morphology, which was mainly attributed to the fact that scaffolds with higher hydrophilicity and WHC could enhance cell adhesion and migration into the inner part of the 3D scaffolds[33]. In addition, the number of cells in AGS7 was significantly higher than that in AGS5, which was attributed to the fact that to a certain extent the cell proliferation capacity was negatively correlated with the degradation rate[34], and a higher degradation

rate might lead to fewer cell adhesion sites and thus affect the cell proliferation behavior. The proliferation curves result of AGS5, AGS7 and AGS10 showed that the linear and parabolic proliferation curves were lower than the normal cell proliferation curves in AGS5 and AGS10, while AGS7 conformed to the normal cell proliferation curves, meanwhile, the cell number of AGS7 was significantly higher than that of AGS5 and AGS10 as shown by the 7$^{th}$ day cell proliferation, which further illustrated that cell proliferation was promoted by AGS7 compared with AGS5 and AGS10. In summary, AGS7 has a lower degradation rate while maintaining higher water-holding capacity. This also implied that more cell adhesion sites could be retained by AGS7 while maintaining efficient nutrient and oxygen exchanges, which had a positive impact on cell attachment, proliferation, and migration in the scaffold.

To further investigate the effect of printing materials on the proliferative state of cells. As shown in Fig. 3B, the cell attachment efficiency of AGS5 and AGS7 was significantly higher than that of AGS10, as revealed by the results on the first day of culture. And based on the cell multiplication time, it was found that AGS5 and AGS7 achieved cell multiplication on the third day and entered the exponential growth period of cell proliferation on the 4$^{th}$ day, consistent with the normal cell proliferation curve. In contrast, AGS10 deviated from the normal cell proliferation curve throughout the entire cell value-added cycle, which was not conducive to the successive cultivation of cells in the later stages. Notably, the linear proliferation curve of AGS5 showed a linear divergence on the 4$^{th}$, suggesting that cell migration and repopulation were limited by the material during proliferation. At the same time as, as shown in Fig. S1, AGS5 was not suitable for building larger structures. This limitation was due to a lack of 3D printing performance and the mechanical properties of the material, leading to structural changes and center collapse when trying to create larger-scale structures. As a result, the study further elucidated the advantages of AGS7 in the process of cell attachment, cell migration, cell proliferation and cell nutrient exchange during the continuous cell culture process through the cell attachment and proliferation in different ratios of materials. Based on these results, the scaffolds prepared from AG7 ink were selected as the scaffolds for subsequent 3D tissue culture.

### 3.4 *Tissue culture of 3D bio-printed scaffolds*

Unlike traditional two-dimensional cultures, 3D culturing of cells in 3D bio-printed tissue constructs mimics the *in vivo* condition of cells, allowing them to grow in three dimensions and restoring the physiological characteristics of natural tissues. The biocompatibility of bio-inks was elucidated through the above studies, and in order to further clarify the performance of the scaffolds, the study was carried out to elucidate the advantages of the scaffolds in 3D cell cultures through a tissue culture process similar to that of organoid cultures. The study first constructed a model of tissue culture, as shown in Fig. 4A, the above-prepared ink (AG7) was mixed with myoblasts cells to prepare bio-ink with a cell concentration of 1 × 10$^5$ cells/mL

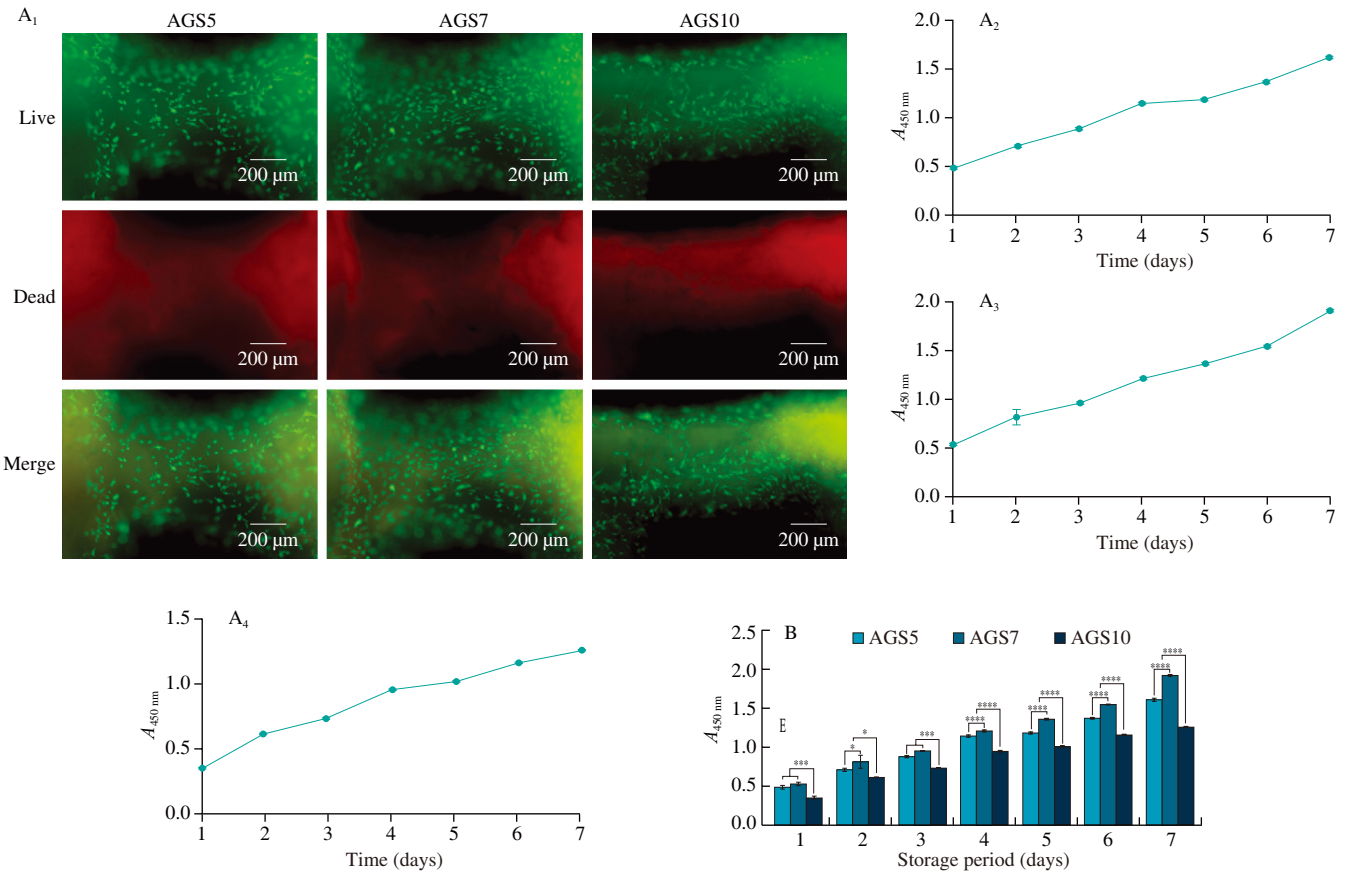


**Fig. 3** Bio-compatibility tests of various scaffolds printed with different inks and myoblast. (A) Fluorescence micrographs of individual scaffolds after live (green) and dead (red) staining on day 7, and cell proliferation curve (1−7 days). ($A_2$) AGS5; ($A_3$) AGS7; ($A_4$) AGS10. (B) Representative absorbance values at 450 nm for each scaffold (1−7 days). Statistical significance was set to ****$P$ < 0.000 1, ***$P$ < 0.001 and *$P$ < 0.05.

for 3D bio-printing. Cell behavior as well as cell proliferation status was further indicated by fluorescence microscopy (1−7 days) and microscopic observation (1−15 days) during scaffold culture. As shown in Fig. 4B, the cells within the scaffold exhibited good proliferation, with a tendency for initial cells to proliferate near the edge of the scaffold after attachment. This phenomenon may be due to the fact that the edge of the scaffold was more favorable for nutrient exchange, which facilitates rapid cell proliferation and migration. On the 7$^{th}$ day, the cells had completely covered the entire scaffold and showed good dispersion, further demonstrating that the scaffolds not only had good biocompatibility but also no significant effect on cell attachment and migration. In addition, no obvious dead cells were observed within the scaffolds at any time point, suggesting that short-term glutaraldehyde cross-linking at low concentrations had no significant effect on the cell state. As shown in Fig. 4C, the number of cells per unit area was analyzed, and it was observed that the scaffolds entered the exponential growth phase of cell proliferation after the 3$^{rd}$, with the number of cells reaching 562 cells/mm$^2$ on the 7$^{th}$ day. As shown in Figs. 4D and S2, cells within the scaffold proliferated rapidly during the first seven days, which was consistent with the above results. Notably, when the cells proliferated continuously up to 9$^{th}$ day, the inner space of the scaffold was filled with cells reaching the growth inhibition of the scaffold, and the cells began to spill out of the scaffold. In addition, cells began to migrate and proliferate at the edge of the scaffold apertures through cell-cell connections. On 11$^{th}$ day, the cell junctions at the edge of the aperture formed a thread-like cell cluster. On 13$^{th}$ day, cells at the edge of the scaffold aperture begin to spread and proliferate in a peripheral direction to form an open membranous morphology cellular organization based on the linear cell clusters. On 15$^{th}$ day, a completely closed membrane morphology cell organization was formed in the aperture of the scaffold. As shown in Fig. 4E, membranous cellular tissue hardly appeared at the edge of the scaffold aperture until the 9$^{th}$ day of cell culture, and the formation of membrane morphology cellular tissue began to accelerate at 11 to

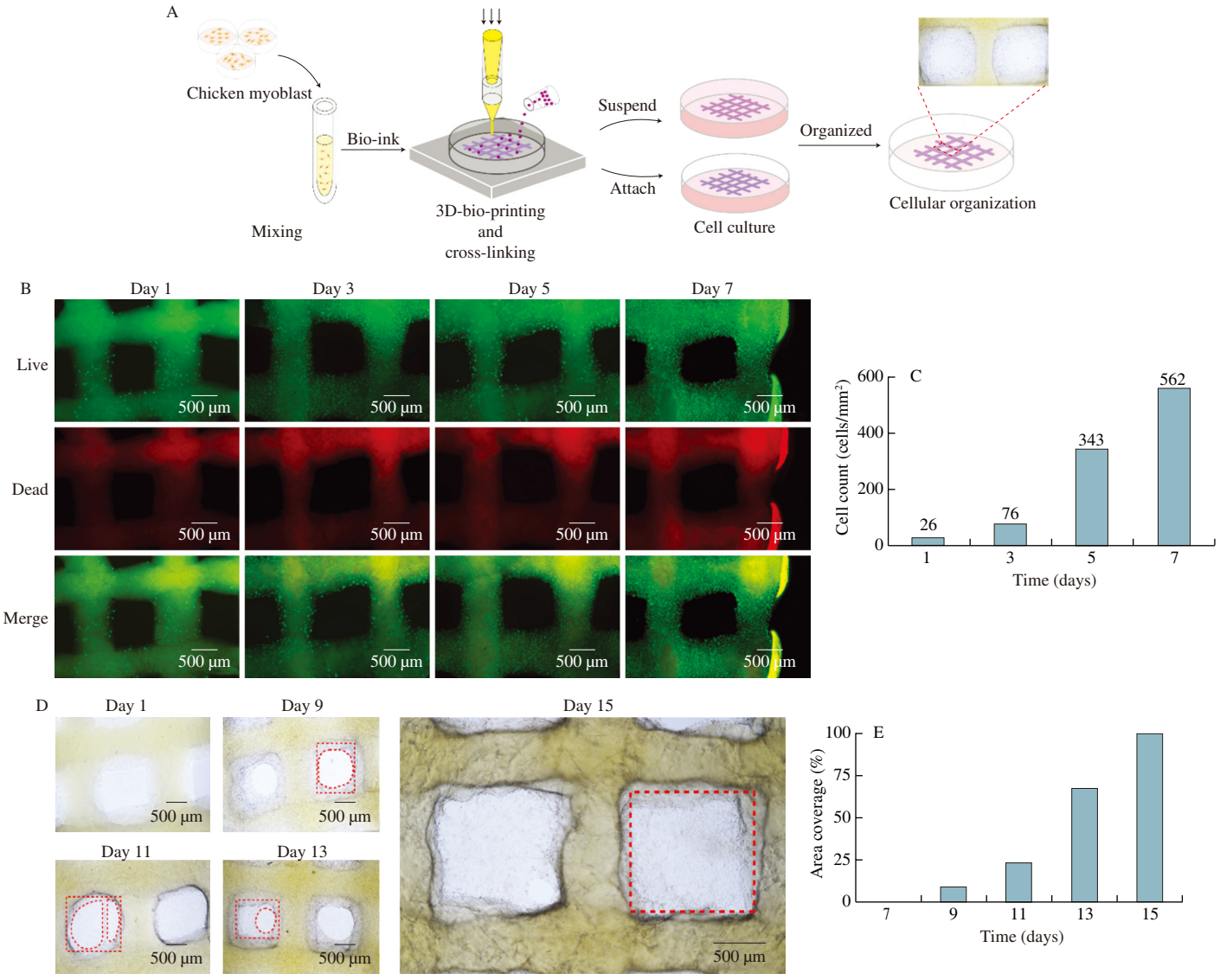


**Fig. 4** Cultivation process of membranous morphology cellular tissues. (A) Schematic diagram of the preparation of bio-inks and the cell culture process of the scaffolds. (B) Fluorescence micrographs of individual scaffolds after live (green) and dead (red) staining on days 1, 3, 5 and 7. (C) Cells per square millimeter. (D) Micrographs of individual scaffolds on days 1, 9, 11, 13 and 15 (inside the red dotted line was membranous morphology cellular tissue). (E) Area of membranous cellular tissue.

15 days with an approximate 75% increase in its area. Therefore, the cells in the scaffold underwent a large amount of proliferation and cell migration in the early stage, and in the middle stage, the cells showed the proliferation of dots and lines in the aperture of the scaffold, and finally completed the formation of membranous cell tissues in the aperture of the scaffold. One of the reasons for the formation of membranous morphology cell tissues was probably due to the fact that the bio-ink, which was mainly composed of polysaccharides and peptides, could mimic the structural features of the extracellular matrix (ECM) *in vivo* and provide excellent micro-environment for cell proliferation and proliferation[35], thus promoting cell proliferation. In addition, cell-cell interactions regulate cell morphology when cell density increased, and higher cell densities promoted cell-cell contacts through the formation of multicellular clusters[36]. As a result, cell-cell interactions and the formation of membranous morphology cellular organization in the aperture may have been facilitated when cell densities at the aperture edges were elevated.

### 3.5 *Differences between 2D and 3D cell culture*

Following the completion of 3D bio-printing, cellular proliferation and migration within the scaffold occurred at an accelerated pace. Within the peripheral regions of the scaffold, cells demonstrate vigorous proliferation and migration, ultimately leading to the formation of linearly aligned cell clusters within the pore regions. These linearly organized cells gradually expand and interconnect, eventually giving rise to a closed, membrane morphology cellular tissue structure. Microscopic observations further validate this process.

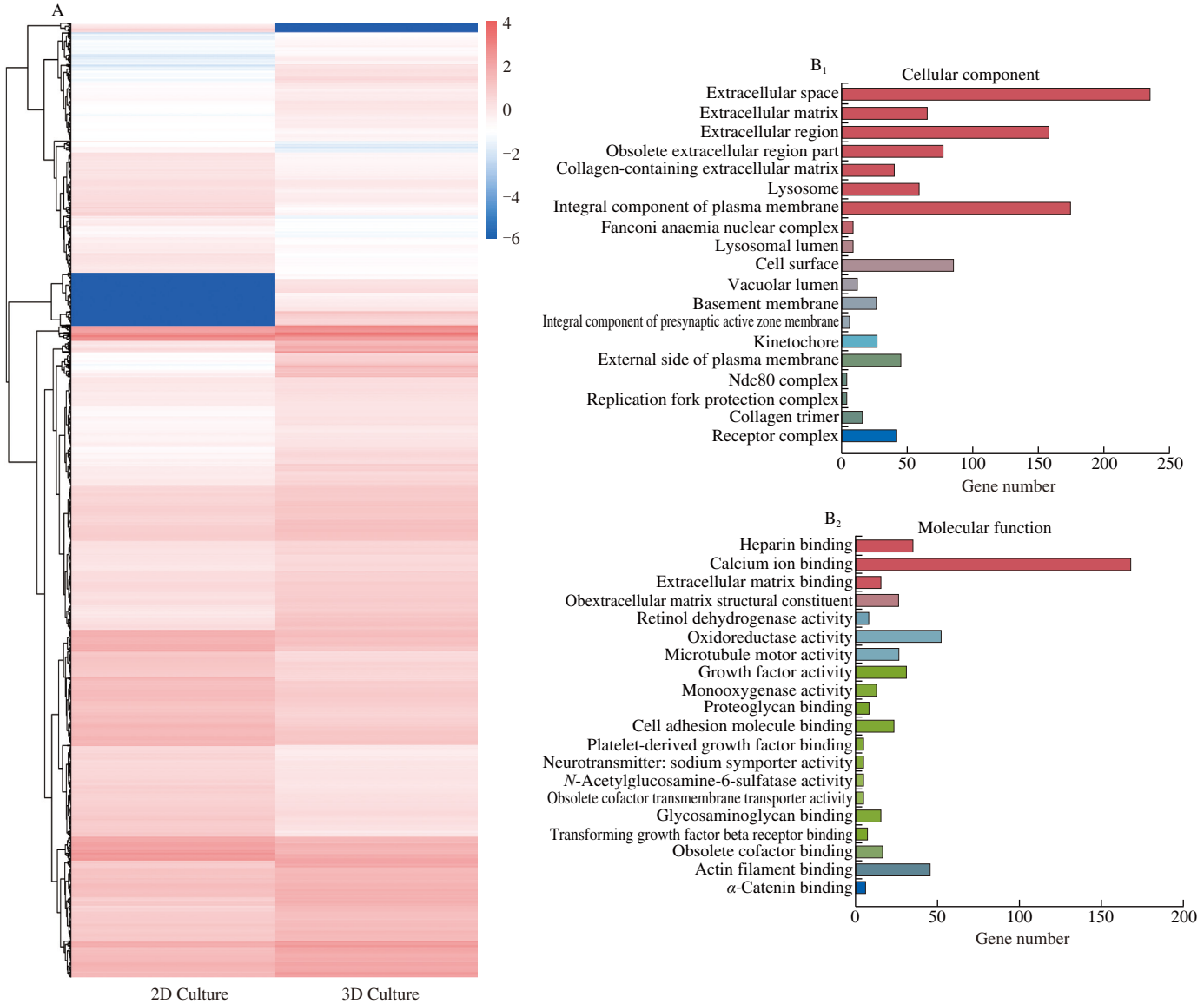


**Fig. 5** Differences between 2D and 3D cell culture. (A) Heat map of gene expression in different cultures. (B) GO functional enrichment of differentially expressed genes. (C) KEGG enrichment pathway analysis of differentially expressed genes. (D) Significance analysis and expression of differentially expressed genes. (E) Quantitative PCR validation of differential genes in 2D and 3D cell cultures. ($E_1$) *Ltpb2*; ($E_2$) *Bmp4*; ($E_3$) *Nid2*; ($E_4$) *Pax7*; ($E_5$) *Myod*; ($E_6$) *Myog*. Statistical significance was set to $^{**}P < 0.01$ and $^{*}P < 0.05$. (F) Fluorescence micrographs results (top: cells in the scaffold; bottom: membranous cell tissue). ($G_1$) Micrographs of early-stage, mid-stage and late-stage cell cultures. Differential expression validation of major genes regulating cell behavior in 3D cell culture at different time periods, ($G_2$) *Cdh20*; ($G_3$) *Dsg2*; ($G_4$) *Megf10*; ($G_5$) *Fgf7*; ($G_6$) *Pax7*; ($G_7$) *Myod*. Statistical significance was set to $^{***}P < 0.001$, $^{**}P < 0.01$ and $^{*}P < 0.05$. Differential expression validation of major genes regulating cell behavior in 3D cell culture at different time periods (early stage, mid stage and late stage). (H) Protein expression analysis of ($H_1$, $H_3$) PAX7 and ($H_2$, $H_4$) MYOD at different stages (early stage and late stage) in the scaffolds. Statistical significance was set to $^{***}P < 0.001$ and $^{**}P < 0.01$.

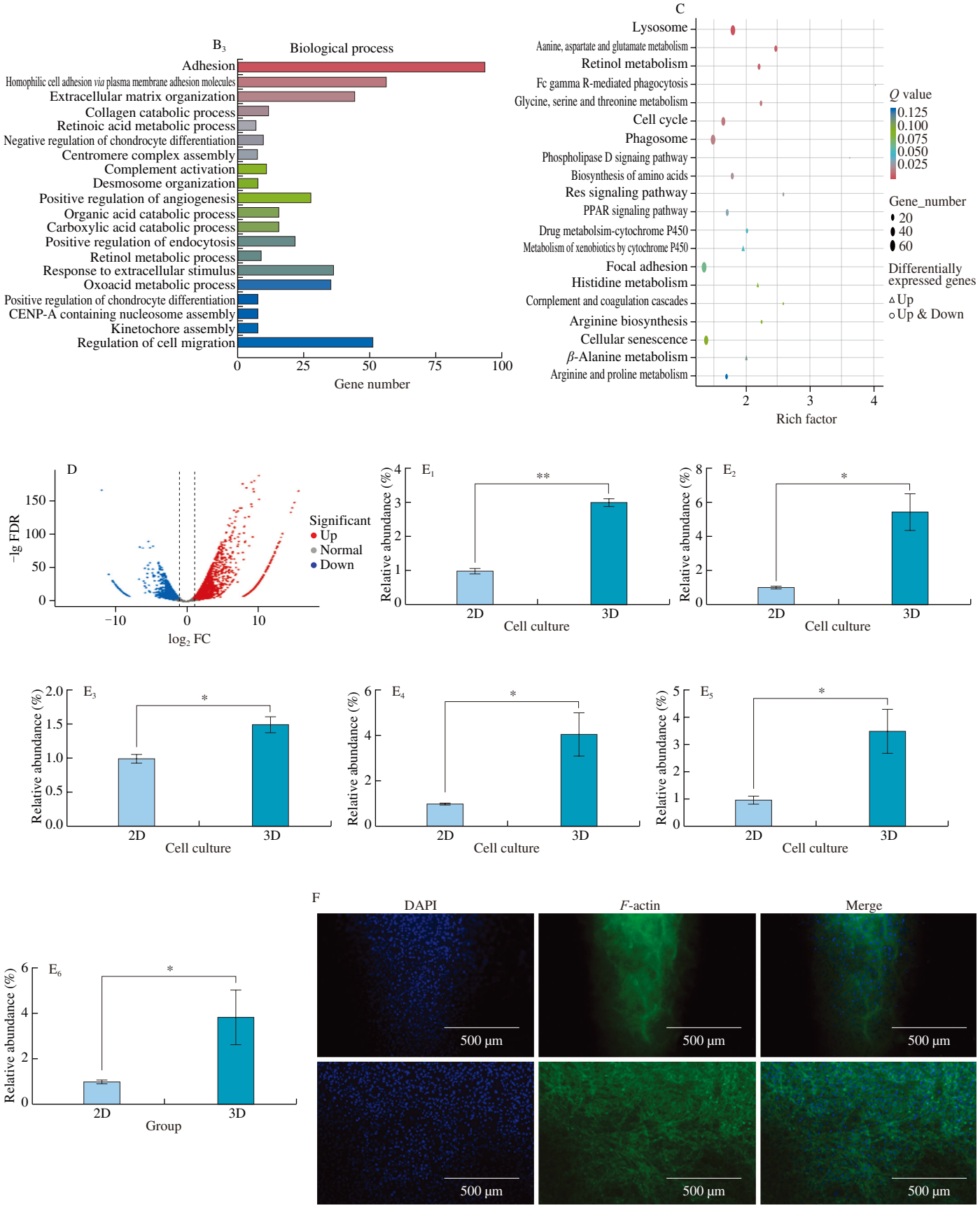


**Fig. 5** (*Continued*)

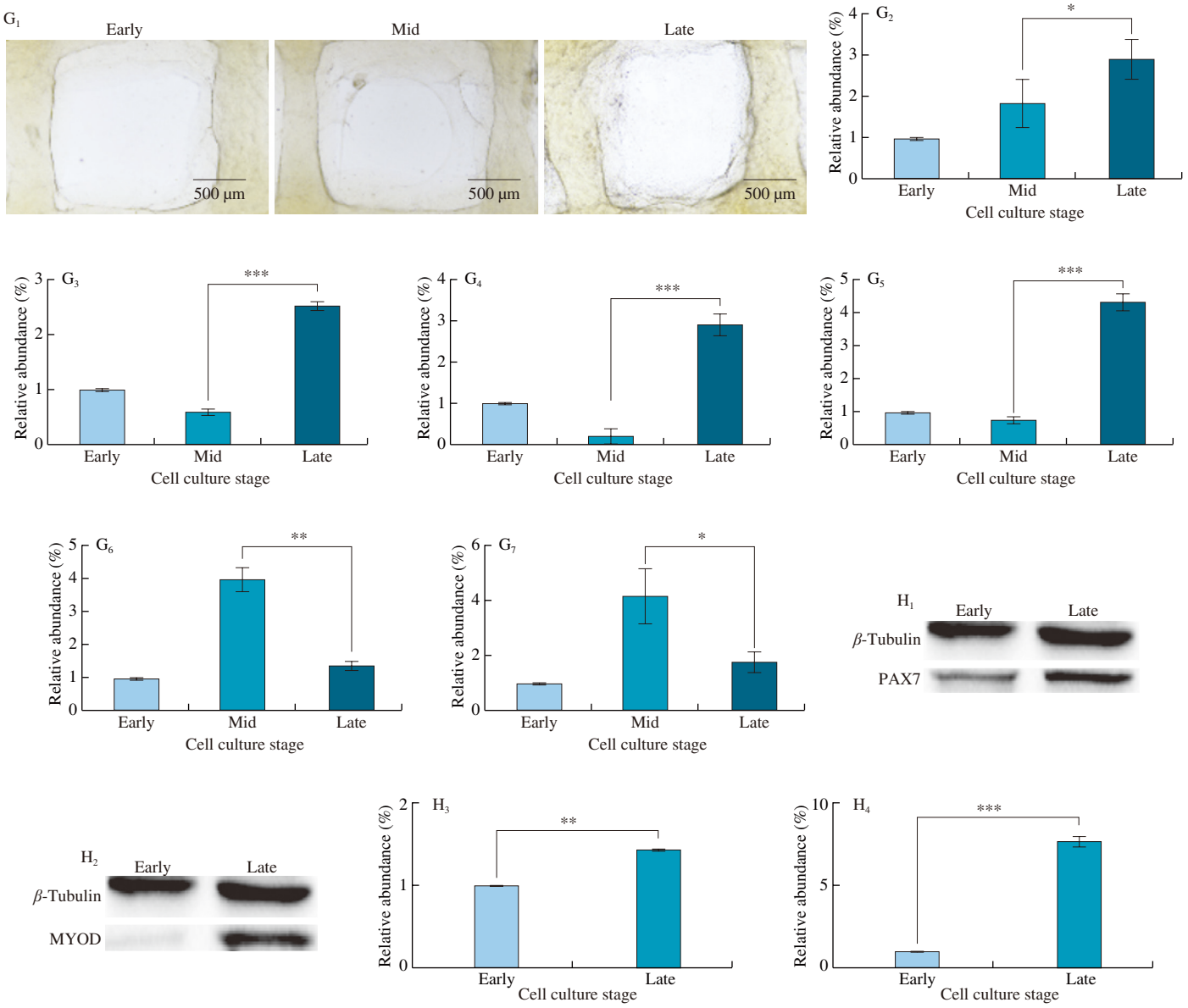


**Fig. 5** (*Continued*)

As shown in Fig. S2, transcriptome sequence analysis, revealed a discernible distinction between 2D cell culture and 3D cell culture, characterized by a correlation coefficient of 0.374. Differential gene analysis revealed 3 559 differentially expressed genes between the 2 culture methods. Venn diagram analysis further revealed overlapping and unique gene expression patterns in 2D and 3D cell cultures. To gain deeper insights into the disparities between 2D and 3D cell cultures, the data from the 2 types of samples were segregated, and a comparative analysis of differential gene expression was performed. Utilizing data from both culture methods, gene clustering heat-map analysis was conducted, as shown in Fig. 5A, revealing genes with divergent expression profiles. As shown in Fig. 5B, GO analysis results unveiled the enrichment of various biological processes, cellular components, and molecular functions associated with cell adhesion, migration, proliferation, and cellular organization. Notably, calcium ion binding, extracellular matrix binding, cell surface, cell adhesion, extracellular matrix structural constituents, and growth factor activity played pivotal roles in these biological processes. Among these functions, differentially expressed genes with substantial up-regulation include *Ltbp2*, *Olfml2b*, *Fbln2*, *Nid2*, *Col3a1*, *Bmp4*, *Fgf7*, *Inhbb*, *Lama4*, *Csta*, *Gpnmb*, *Nfasc*, *Npy2r*, *Bmp7*, *Megf10*, *Cdh20*, *Clstn2*, *Bnc1*, *Dsg2*, etc., furthermore, *Ltbp2*, *Col3a1*, and *Cdh20* genes were closely associated with cell adhesion[37-38], while *Bmp4* and *Bmp7* are growth factors implicated in cell proliferation[39]. Hence, it is posited that the expression of these genes was enhanced during cell adhesion and proliferation processes by 3D-printed scaffold materials, thereby improving outcomes in cell adhesion and proliferation. The main function of "homophilic cell adhesion *via* plasma membrane adhesion molecules and desmosome organization in the enrichment results was achieving cell attachment and contributing to intercellular adhesion as well as inter-cellular junctions through the same adhesion molecules on the plasma membrane. Additionally, a key role in mediating intercellular junctions and stability was played by the highly expressed genes, *Dsg2c*, and *Cdh20*[40]. Therefore, it was hypothesized that an important contribution to the formation of 3D cellular tissue structures could be

made by 3D printed scaffold materials. In the pursuit of a more comprehensive understanding of the disparities between 2D and 3D cell cultures, KEGG pathway analysis was employed. Our analysis outcomes underscore the substantial enrichment of the focal adhesion and cell cycle signaling pathways. As shown in Figs. 5C and S3, visually represents the enrichment of 68 regulatory genes in the Focal adhesion pathway, 59 genes in the regulation of actin cytoskeleton pathway, 43 genes in the cell cycle pathway, 33 genes in the tight junction pathway, 54 genes in the cell adhesion molecules pathway, and 57 genes in the calcium signaling pathway. The core functions of the focal adhesion/regulation of actin cytoskeleton/cell cycle signaling pathways revolved around facilitating cell adhesion, proliferation, and migration. On the other hand, the principal role of the tight junction/cell adhesion molecules pathways was to mediate cell adhesion and intercellular interactions, thus establishing crucial tight connections between cells that were indispensable for tissue development and the preservation of tissue integrity. As shown in Fig. 5D, the primary differentially expressed genes between the 2 cultivation methods, namely, *Abi3bp*, *Cd36*, *Gpnmb*, *Apoa1*, *Ly6e*, *Csta*, *Rln1*, *Loc430862*, and *Hps5*. These genes played pivotal roles in governing cell migration, adhesion, and proliferation within the context of signaling pathways. In addition, to further explored the effect of 3D culture on the expression of key genes regulating cell migration, attachment and proliferation, as shown in Fig. 5E, qRT-PCR results showed that *Ltbp2*, *Nid2*, *Bmp4*, *Pax7*, *Myod* and *Myog* genes showed higher expression in 3D cell culture. Among them, the genes of *Ltbp2* and *Nid2* mainly affected cell adhesion as well as migration, *Pax7*, *Bmp4* and *Myod* maintained high expression levels mainly in cell division, while *Myog* was important for cellular organization formation[41]. It was demonstrated that 3D culture could promote the expression of key genes and thus have a positive effect on cell proliferation, adhesion, and cellular organization formation. These results aligned with the transcriptome analysis findings. As shown in Fig. 5F, immunity fluorescence results at the later stage of 3D scaffold culture showed that the entire scaffold had been covered by the cells, and multilayered membranous cellular tissues with cell-to-cell connections were formed in the scaffold apertures. To further validate the effect of 3D printed scaffolds on cellular adherence and the formation of membrane morphology cellular tissues, as shown in Fig. 5G, cell growth in the scaffolds was divided into three phases, with the first phase being the cellular adherence in the scaffolds after completion of the bio-printing, the middle phase being the cellular proliferation within the scaffolds, and the later phase being the formation of membrane cellular tissues in the apertures of the scaffolds. The qRT-PCR results showed enhanced expression of genes (both *Cdh20*, *Dsg2* and *Megf10*) affecting cell adhesion and tissue formation. Among them, the main roles of *Cdh20*, *Dsg2* and *Megf10* were involved in cell adhesion and inter-cellular junctions[42-43], and it was noteworthy that the expression of *Cdh20* was persistently high while the expression of *Dsg2* and *Megf10* was significantly increased only in the late stage. Therefore, it is inferred that *Cdh20* not only played an important role in cell adhesion in the early stage but also positively influenced the formation of membranous cellular tissues with *Dsg2* and *Megf10* in the late stage. During cell division *Pax7* was highly expressed and *Myod* gene expression level increased, while during cell alignment *Pax7* was no longer expressed or was expressed at a very low level, and *Myod* expression level was also significantly reduced[44]. However, the PCR results showed that the expression levels of *Pax7* and *Myod* were significantly higher than those in the early stage of the scaffold, which also proved that the cells did not stop dividing in the late stage of the formation of organization, continued to proliferate in the aperture of the scaffold, and then generated multilayered membranous cellular tissues. The high expression of *Fgf7* in the late stage of the scaffold also indicated that the cells did not stop proliferating in the late stage of the scaffold. As shown in Fig. 5H, the Western blot results showed a significant increase in the expression of PAX7 and MYOD proteins in the later stage compared with the earlier stage. Furthermore, PAX7 was considered a marker for muscle stem cells, and its expression was deemed essential during muscle regeneration processes, where it played a crucial role in regulating the growth, maintenance, and repair of mature muscle fibers[45]. MYOD played a role in myoblast myogenic differentiation and was used to induce the differentiation of premyoblasts into myoblasts[46-47]. Therefore, the relatively high expression of PAX7 and MYOD in the later stages suggested that the proliferative behavior of cells within the scaffold had not ceased, while cells were possibly preparing for differentiation and muscle tissue formation, which was consistent with the gene expression results and transcriptomic results. Thus, the bio-inks composed of albumen and gelatin not only exhibited good biocompatibility, but also positively influenced the expression of key genes regulating cell adhesion and proliferation in the cells within the scaffolds and induced the formation of membranous morphology cellular tissues, demonstrating their potential as scaffolds for cellular organizing cultures of cultivated meat.

### *3.6 Scaffold suspension and adherent culture*

The proliferation of cells in the scaffold was more specific than in traditional culture dishes. In order to further explore cell adhesion, proliferation, the formation of tissue-like cell groups in 3D scaffolds, and to simulate the micro-environment of 3D cell growth *in vivo*, a study on scaffold-adherent culture and scaffold suspension culture was conducted. The data from 2 samples were analyzed, and differential gene comparison analysis was conducted. As shown in Fig. 6A, based on the data from these 2 culture methods, gene clustering heat map analysis was performed, revealing genes with differential expression. As shown in Figs. 6B and S4, the main enriched function in the GO results include extracellular space, microtubule motor activity, microtubule binding, kinesin complex, and collagen-containing extracellular matrix. These functions played a role in maintaining cell morphology, cell movement, intracellular substance transport, and cell adhesion in various biological processes. This may suggest significant differences in the composition and interactions of extracellular matrix, cell signaling, and the extracellular environment in suspension culture samples. As shown in Figs. 6C and S4, KEGG enrichment results indicated significant enrichment in focal adhesion, cell cycle, thyroid hormone signaling pathway, and fanconi additionally. In addition, as shown in Fig. S4, 16 genes were enriched in the MAPK signaling pathway, 12 genes were enriched in cell cycle, while 8 genes were enriched in the Tgf-β signaling pathway and Wnt signaling pathway. As shown in Fig. 6D, differential genes between the 2 culture methods included *Lgr5*, *Col9a*, *Map3k8*, *Fgf16*, *Nog*, *Cdk1*, *Ttk*, *Aaed1*, *Rcan2*, *Fancb*, *Fancf*, *Brca2*, and more. Low expression of the

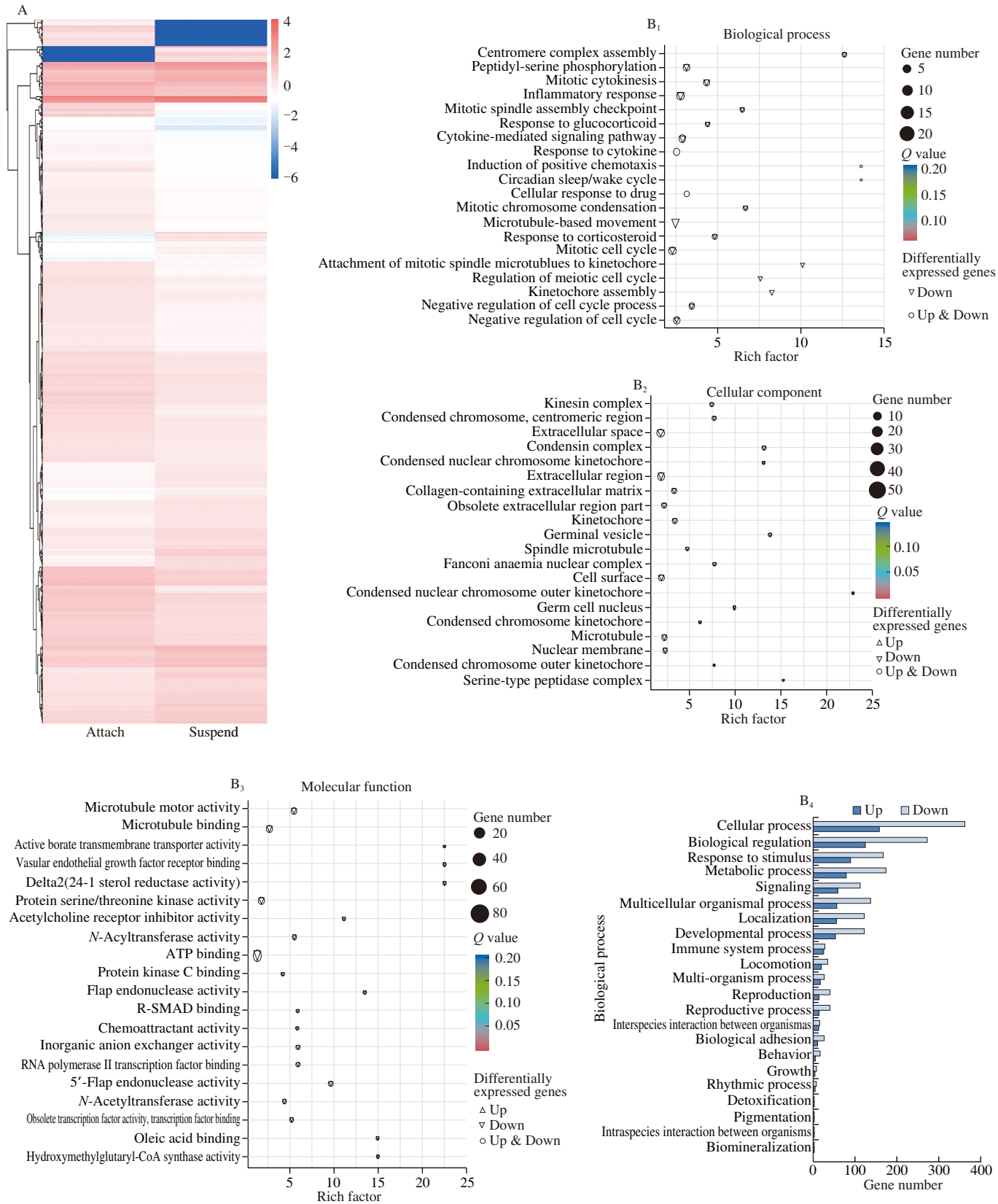


**Fig. 6** Differences between scaffold suspension and adherent culture. (A) Heat map of gene expression in different cultures. (B) GO function enrichment of differentially expressed genes. (C) KEGG enrichment pathway analysis. (D) Results of relative expression of differentially expressed genes. (E) Differential expression validation of major genes regulating cell behavior in 3D cell culture (attach culture and suspend culture) at different time periods (1, 4, 7, 10: early stage; 2, 5, 8, 11: mid stage; 3, 6, 9, 12: late stage). ($E_1$-$E_3$) *Cdk1*; ($E_4$-$E_6$) *Ttk*; ($E_7$-$E_9$) *Lgr5*; ($E_{10}$-$E_{12}$) *Map3k8*. Statistical significance was set to $^{****}P < 0.000\ 1$, $^{***}P < 0.001$, $^{**}P < 0.01$ and $^{*}P < 0.05$.

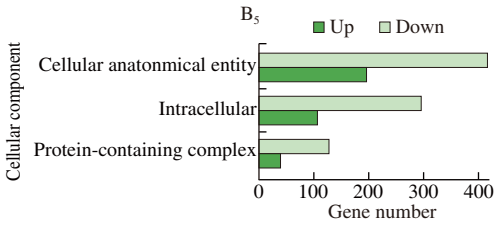


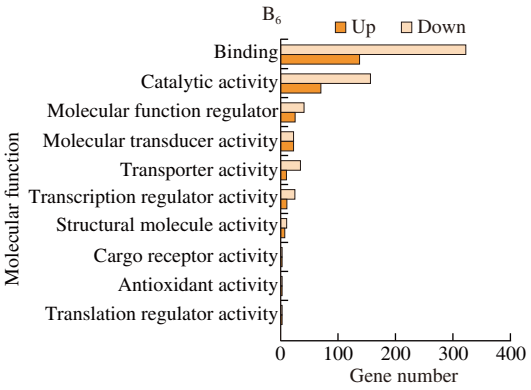


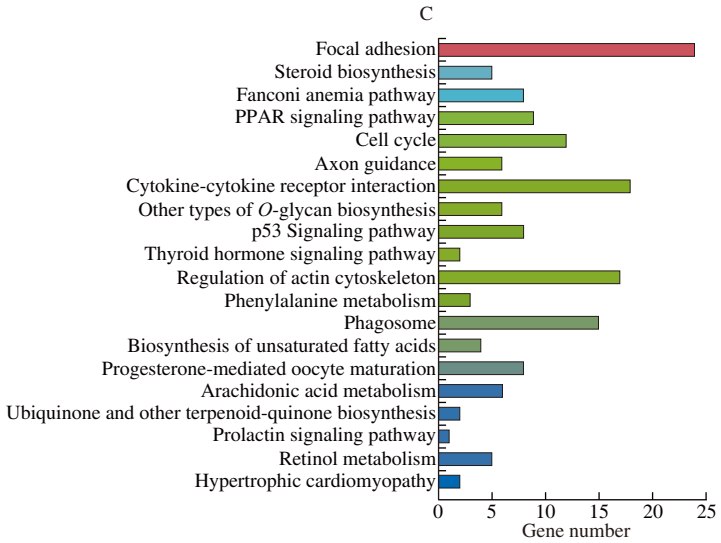


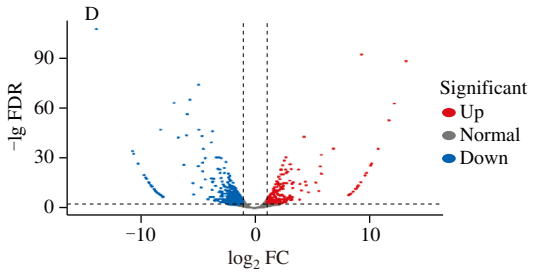


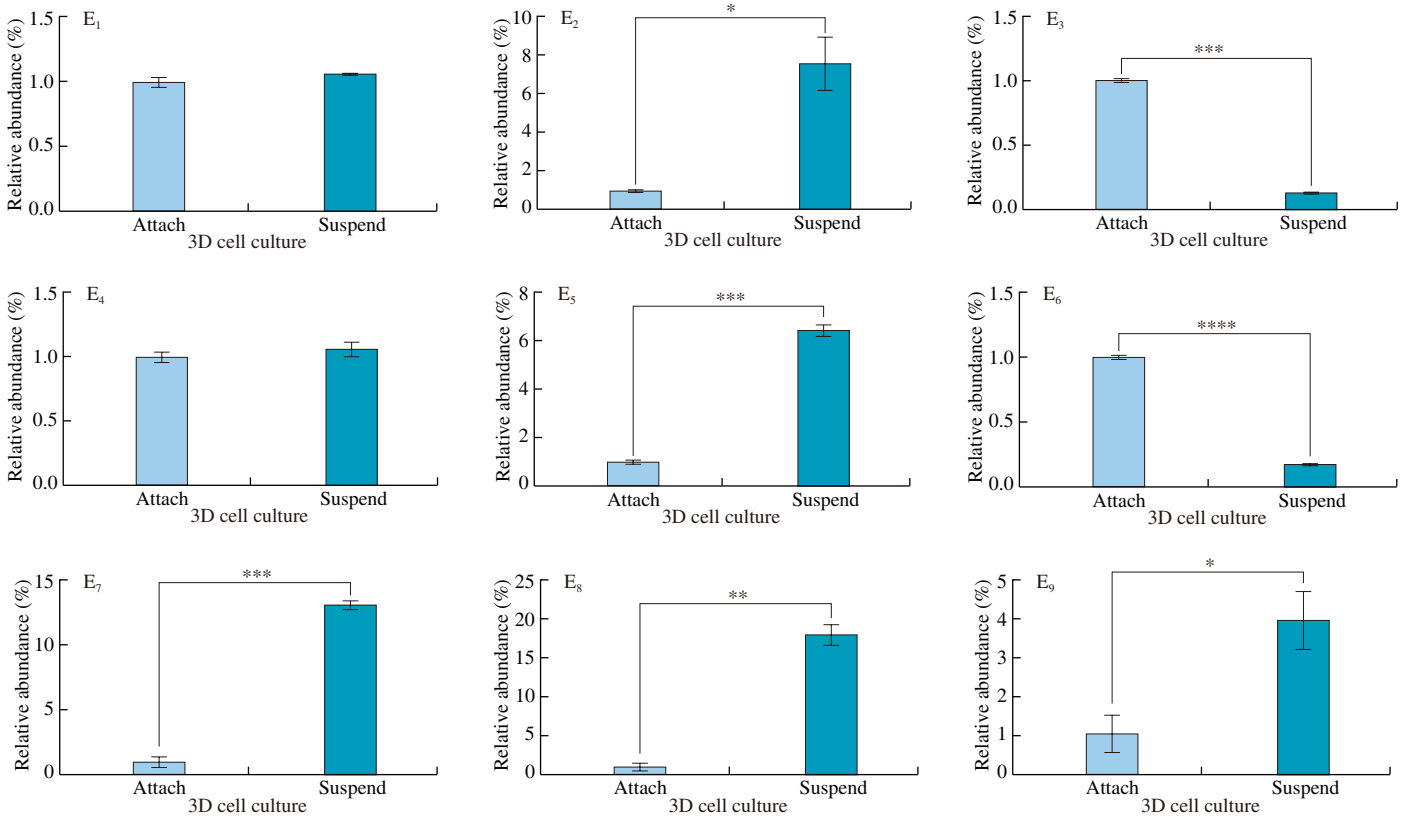


**Fig. 6** (*Continued*)

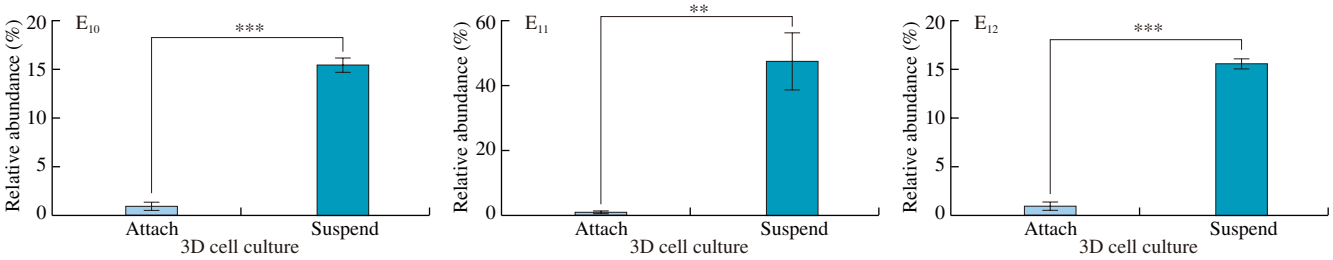


**Fig. 6** (*Continued*)

*Cdk1* and *Ttk* gene could potentially hinder cell proliferation, while high expression of *Lgr5*, *Map3k8* and *Nog* genes may indicate that the cells have potential for differentiation. From this, it can be observed that the shorter proliferation cycle of suspension-cultured cells allowed for earlier entry into later stages of tissue culture compared to scaffold-adherent cultures, and greater potential in terms of differentiation potential might be exhibited by suspension cultures. As shown in Fig. 6E, the qRT-PCR results indicated that the expression of *Cdk1* and *Ttk* was significantly increased in the middle and decreased in the late stage, and the expression of both *Lgr5* and *Map3k8* genes was high. It was demonstrated that cells in suspension scaffolds were more active in mitosis before forming membrane morphology cellular tissues. The lower expression of *Cdk1* and *Ttk* at a later stage also suggested that the later stage of tissue culture might be entered earlier by suspension cultures[48-49]. In addition, the relatively high expression of *Lgr5* and *Map3k8* may affect the Wnt/MAPK signaling pathway[50], which functions to terminate cell division and initiate cell differentiation[51], thus, cells in suspension cultures with relatively high activity of the Wnt/MAPK signaling pathway were more likely to undergo cell differentiation. In summary, in order to better simulate the growth environment of cells *in vivo* and try to break through the limitations of traditional adherent culture, we conducted a preliminary study of suspension scaffold culture. The results showed that there were significant differences between the 2 deposits in terms of cell proliferation, attachment, motility and differentiation, especially in cell proliferation and differentiation, which will be the focus of future research.

## 4. Conclusion

In summary, with the aim of producing printability bio-inks for cell cultured meat tissue applications, we developed novel bio-inks composed of albumen and gelatin. 3D-printed scaffolds were successfully produced, and morphology, water absorption, printing performance, degradability, and biological compatibility were characterized. AG7 demonstrated better printability, at the same time S-shaped exponential growth curve further revealed the significant advantages of AGS7 scaffolds in cell culture. The results of cell culture indicated that effective adhesion, proliferation, and migration of myoblasts occurred in the scaffolds. More importantly, a muscle cell organization similar to organoid culture was achieved through 3D cell culture. In addition, obvious differences between 2D culture and 3D culture in the processes of cell attachment, proliferation, and migration were revealed by transcriptomics, qRT-PCR, and Western bolt analysis results. Simultaneously, the promotion of gene expression related to cell-cell connections (*Cdh20*, *Dsg2*, and *Megf10*) was observed in 3D culture, contributing to the formation of cell tissue. Overall, the possibility of a new method for manufacturing cultured meat was revealed by this study, indicating that 3D cell culture has great application potential in the field of cell-cultured meat.

## Declaration of competing interest

The authors declare that they have no known competing financial interests or personal relationships that could have appeared to influence the work reported in this paper.

## Acknowledgements

This work was funded under the National key research and development plan (2021YFC2101400), Chinese Academy of Engineering Strategic Research and Consulting Project (2023-XZ-79, 2022-30-19), National Natural Science Foundation of China (22005019).

## Appendix A. Supplementary data

Supplementary data associated with this article can be found, in the online version, at http://doi.org/10.26599/FSHW.2024.9250249.

### References

[1] C. Bomkamp, S.C. Skaalure, G.F. Fernando, et al., Scaffolding biomaterials for 3D cultivated meat: prospects and challenges, Adv. Sci. 9 (2022) 2102908. https://doi.org/10.1002/advs.202102908.

[2] Y. Chen, L. Li, L. Chen, et al., Gellan gum-gelatin scaffolds with $Ca^{2+}$ crosslinking for constructing a structured cell cultured meat model, Biomaterials 299 (2023) 122176. https://doi.org/10.1016/j.biomaterials.2023.122176.

[3] I. Ianovici, Y. Zagury, I. Redenski, et al., 3D-printable plant protein-enriched scaffolds for cultivated meat development, Biomaterials 284 (2022) 121487. https://doi.org/10.1016/j.biomaterials.2022.121487.

[4] A. Zernov, L. Baruch, M. Machluf, Chitosan-collagen hydrogel microparticles as edible cell microcarriers for cultured meat, Food Hydrocoll. 129 (2022) 107632. https://doi.org/10.1016/j.foodhyd.2022.107632.

[5] S. Park, S. Jung, M. Choi, et al., Gelatin MAGIC powder as nutrient-delivering 3D spacer for growing cell sheets into cost-effective cultured meat, Biomaterials 278 (2021) 121155. https://doi.org/10.1016/j.biomaterials.2021.121155.

[6] J.S.H. Seah, S. Singh, L.P. Tan, et al., Scaffolds for the manufacture of cultured meat, Crit. Rev. Biotechnol. 42 (2022) 311-323. https://doi.org/10.1080/07388551.2021.1931803.

[7] Y. Wang, J. Li, Y. Li, et al., Biomimetic bioinks of nanofibrillar polymeric hydrogels for 3D bioprinting, Nano Today 39 (2021) 101180. https://doi.org/10.1016/j.nantod.2021.101180.

[8] B. Grigoryan, S.J. Paulsen, D.C. Corbett, et al., Multivascular networks and functional intravascular topologies within biocompatible hydrogels, Science 364 (2019) 458-464. https://doi.org/10.1126/science.aav9750.

[9] S. Im, G. Choe, J.M. Seok, et al., An osteogenic bioink composed of alginate, cellulose nanofibrils, and polydopamine nanoparticles for 3D bioprinting and bone tissue engineering, Int. J. Biol. Macromol. 205 (2022) 520-529. https://doi.org/10.1016/j.ijbiomac.2022.02.012.

[10] H.W. Kang, S.J. Lee, I.K. Ko, et al., A 3D bioprinting system to produce human-scale tissue constructs with structural integrity, Nat. Biotechnol. 34 (2016) 312-319. https://doi.org/10.1038/nbt.3413.

[11] A. Lee, A. Hudson, D. Shiwarski, et al., 3D bioprinting of collagen to rebuild components of the human heart, Science 365 (2019) 482-487. https://doi.org/10.1126/science.aav9051.

[12] X. Ma, X. Qu, W. Zhu, et al., Deterministically patterned biomimetic human iPSC-derived hepatic model *via* rapid 3D bioprinting, Proc. Nat. Acad. Sci. 113 (2016) 2206-2211. https://doi.org/10.1073/pnas.1524510113.

[13] Z. Lin, M. Wu, H. He, et al., 3D printing of mechanically stable calcium-free alginate-based scaffolds with tunable surface charge to enable cell adhesion and facile biofunctionalization, Adv. Funct. Mater. 29 (2019) 1808439. https://doi.org/10.1002/adfm.201808439.

[14] X. Dong, Y.Q. Zhang, An insight on egg white: from most common functional food to biomaterial application, J. Biomed. Mater. Res. Part B Appl. Biomater. 109 (2021) 1045-1058. https://doi.org/10.1002/jbm.b.34768.

[15] W. Mizunoya, A. Tashima, Y. Sato, et al., The growth-promoting activity of egg white proteins in the C2C12 myoblast cell line, Anim. Sci. J. 86 (2015) 194-199. https://doi.org/10.1111/asj.12257.

[16] K. Huang, J. Hou, Z. Gu, et al., Egg-white-/eggshell-based biomimetic hybrid hydrogels for bone regeneration, Biomater. Sci. Eng. 5 (2019) 5384-5391. https://doi.org/10.1021/acsbiomaterials.9b00990.

[17] Y. Delkash, M. Gouin, T. Rimbeault, et al., Bioprinting and *in vitro* characterization of an eggwhite-based cell-laden patch for endothelialized tissue engineering applications, J. Funct. Biomater. 12 (2021) 45. https://doi.org/10.3390/jfb12030045.

[18] Q. Chang, M.A. Darabi, Y. Liu, et al., Hydrogels from natural egg white with extraordinary stretchability, direct-writing 3D printability and self-healing for fabrication of electronic sensors and actuators, J. Mater. Chem. A 7 (2019) 24626-24640. https://doi.org/10.1039/C9TA06233E.

[19] L. Guo, X. Niu, X. Chen, et al., 3D direct writing egg white hydrogel promotes diabetic chronic wound healing *via* self-relied bioactive property, Biomaterials 282 (2022) 121406. https://doi.org/10.1016/j.biomaterials.2022.121406.

[20] X. Wang, Y. Ma, X. Niu, et al., Direct three-dimensional printed egg white hydrogel wound dressing promotes wound healing with hitching adipose stem cells, Front. Bioeng. Biotechnol. 10 (2022) 930551. https://doi.org/10.3389/fbioe.2022.930551.

[21] Q. Li, S. Xu, Q. Feng, et al., 3D printed silk-gelatin hydrogel scaffold with different porous structure and cell seeding strategy for cartilage regeneration, Bioact. Mater. 6 (2021) 3396-3410. https://doi.org/10.1016/j.bioactmat.2021.03.013.

[22] A. Mondal, A. Gebeyehu, M. Miranda, et al., Characterization and printability of Sodium alginate-gelatin hydrogel for bioprinting NSCLC co-culture, Sci. Rep. 9 (2019) 19914. https://doi.org/10.1038/s41598-019-55034-9.

[23] J. Yin, M. Yan, Y. Wang, et al., 3D bioprinting of low-concentration cell-laden gelatin methacrylate (GelMA) bioinks with a two-step cross-linking strategy, ACS Appl. Mater. Interfaces 10 (2018) 6849-6857. https://doi.org/10.1021/acsami.7b16059.

[24] A. Maihemuti, H. Zhang, X. Lin, et al., 3D-printed fish gelatin scaffolds for cartilage tissue engineering, Bioact. Mater. 26 (2023) 77-87. https://doi.org/10.1016/j.bioactmat.2023.02.007.

[25] B. Piola, M. Sabbatini, S. Gino, et al., 3D bioprinting of gelatin-xanthan gum composite hydrogels for growth of human skin cells, Int. J. Mol. Sci. 23 (2022) 539. https://doi.org/10.3390/ijms23010539.

[26] T. Furuike, T. Chaochai, T. Okubo, et al., Fabrication of nonwoven fabrics consisting of gelatin nanofibers cross-linked by glutaraldehyde or *N*-acetyl-*d*-glucosamine by aqueous method, Int. J. Biol. Macromol. 93 (2016) 1530-1538. https://doi.org/10.1016/j.ijbiomac.2016.03.053.

[27] S.A. Poursamar, A.N. Lehner, M. Azami, et al., The effects of crosslinkers on physical, mechanical, and cytotoxic properties of gelatin sponge prepared *via in-situ* gas foaming method as a tissue engineering scaffold, Materials Science and Engineering: C 63 (2016) 1-9. https://doi.org/10.1016/j.msec.2016.02.034.

[28] L. Sun, B. Li, D. Yao, et al., Effects of cross-linking on mechanical, biological properties and biodegradation behavior of *Nile tilapia* skin collagen sponge as a biomedical material, J. Mech. Behav. Biomed. Mater. 80 (2018) 51-58. https://doi.org/10.1016/j.jmbbm.2018.01.006.

[29] H. Mahnama, S. Dadbin, M. Frounchi, et al., Preparation of biodegradable gelatin/PVA porous scaffolds for skin regeneration, Artif. Cells Nanomed. Biotechnol. 45 (2017) 928-935. https://doi.org/10.1080/21691401.2016.1193025.

[30] Y. He, C. Wang, C. Wang, et al., An overview on collagen and gelatin-based cryogels: fabrication, classification, properties and biomedical applications, Polymers 13 (2021) 2299. https://doi.org/10.3390/polym13142299.

[31] I. Bružauskaitė, D. Bironaitė, E. Bagdonas, et al., Scaffolds and cells for tissue regeneration: different scaffold pore sizes—different cell effects, Cytotechnology 68 (2016) 355-369. https://doi.org/10.1007/s10616-015-9895-4.

[32] L. Li, L. Chen, X. Chen, et al., Chitosan-sodium alginate-collagen/gelatin three-dimensional edible scaffolds for building a structured model for cell cultured meat, Int. J. Biol. Macromol. 209 (2022) 668-679. https://doi.org/10.1016/j.ijbiomac.2022.04.052.

[33] S.N. Kalva, Y.B. Dalvi, N. Khanam, et al., Air-jet spun PHBV/PCL blend tissue engineering scaffolds exhibit improved mechanical properties and cell proliferation, Results Mater. 19 (2023) 100415. https://doi.org/10.1016/j.rinma.2023.100415.

[34] H.J. Sung, C. Meredith, C. Johnson, et al., The effect of scaffold degradation rate on three-dimensional cell growth and angiogenesis, Biomaterials 25 (2004) 5735-5742. https://doi.org/10.1016/j.biomaterials.2004.01.066.

[35] S. Sant, D.F. Coutinho, A.K. Gaharwar, et al., Self-assembled hydrogel fiber bundles from oppositely charged polyelectrolytes mimic micro-/nanoscale hierarchy of collagen, Adv. Funct. Mater. 27 (2017) 1606273. https://doi.org/10.1093/hmg/ddx189.

[36] J. Zhang, E. Wehrle, P. Adamek, et al., Optimization of mechanical stiffness and cell density of 3D bioprinted cell-laden scaffolds improves extracellular matrix mineralization and cellular organization for bone tissue engineering, Acta Biomater. 114 (2020) 307-322. https://doi.org/10.1016/j.actbio.2020.07.016.

[37] P. Vehviläinen, M. Hyytiäinen, J. Keski-Oja, Latent transforming growth factor-*β*-binding protein 2 is an adhesion protein for melanoma cells, J. Biol. Chem. 278 (2003) 24705-24713. https://doi.org/10.1074/jbc.M212953200.

[38] J.K. Kim, Y. Xu, X. Xu, et al., A novel binding site in collagen type III for integrins α1β1 and α2β1, J. Biol. Chem. 280 (2005) 32512-32520. https://doi.org/10.1074/jbc.M502431200.

[39] M. Friedrichs, F. Wirsdöerfer, S.B. Flohé, et al., BMP signaling balances proliferation and differentiation of muscle satellite cell descendants, BMC Cell Biol. 12 (2011) 1-17. https://doi.org/10.1186/1471-2121-12-26.

[40] S. Charrasse, F. Comunale, S. De Rossi, et al., Rab35 regulates cadherin-mediated adherens junction formation and myoblast fusion, Mol. Biol. Cell 24 (2013) 234-245. https://doi.org/10.1091/mbc.e12-02-0167.

[41] J. von Maltzahn, A.E. Jones, R.J. Parks, et al., Pax7 is critical for the normal function of satellite cells in adult skeletal muscle, PNAS 110 (2013) 16474-16479. https://doi.org/10.1073/pnas.1307680110.

[42] F. Cooper, A.M. Overmiller, A. Loder, et al., Enhancement of cutaneous wound healing by Dsg2 augmentation of uPAR secretion, J. Invest. Dermatol. 138 (2018) 2470-2479. https://doi.org/10.1016/j.jid.2018.04.024.

[43] M. Saha, S. Mitsuhashi, M.D. Jones, et al., Consequences of MEGF10 deficiency on myoblast function and Notch1 interactions, Hum. Mol. Genet. 26 (2017) 2984-3000.

[44] S. Kuang, M.A. Rudnicki, The emerging biology of satellite cells and their therapeutic potential, Trends Mol. Med. 14 (2008) 82-91. https://doi.org/10.1016/j.molmed.2007.12.004.

[45] S. Oustanina, G. Hause, T. Braun, Pax7 directs postnatal renewal and propagation of myogenic satellite cells but not their specification, EMBO J. 23 (2004) 3430-3439. https://doi.org/10.1038/sj.emboj.7600346.

[46] Q. Wei, B.M. Paterson, Regulation of MyoD function in the dividing myoblast, FEBS Lett. 490 (2001) 171-178. https://doi.org/10.1016/S0014-5793(01)02120-2.

[47] R. Wang, F. Chen, Q. Chen, et al., MyoD is a 3D genome structure organizer for muscle cell identity, Nat. Commun. 13 (2022) 205. https://doi.org/10.1038/s41467-021-27865-6.

[48] D. Santamarıa, C. Barriere, A. Cerqueira, et al., Cdk1 is sufficient to drive the mammalian cell cycle, Nature 448 (2007) 811-815. https://doi.org/10.1038/nature06046.

[49] G.B. Mills, R. Schmandt, M. McGill, et al., Expression of TTK, a novel human protein kinase, is associated with cell proliferation, J. Biol. Chem. 267 (1992) 16000-16006. https://doi.org/10.1016/S0021-9258(19)49633-6.

[50] C. Leung, K.B.A. Murad, A.L.T. Tan, et al., Lgr5 marks adult progenitor cells contributing to skeletal muscle regeneration and sarcoma formation, Cell Rep. 33 (2020) 108535. https://doi.org/10.1016/j.celrep.2020.108535.

[51] J. von Maltzahn, N.C. Chang, C.F. Bentzinger, et al., Wnt signaling in myogenesis, Trends Cell Biol. 22 (2012) 602-609. https://doi.org/10.1016/j.tcb.2012.07.008.